J|A|C|S
ARTICLES

Published on Web 01/12/2010

Probing *E*/*Z* Isomerization on the $C_{10}H_8$ Potential Energy Surface with Ultraviolet Population Transfer Spectroscopy

Josh J. Newby, Christian W. Müller, Ching-Ping Liu,† and Timothy S. Zwier*

Department of Chemistry, Purdue University, West Lafayette, Indiana 47907-2084

Received September 23, 2009; E-mail: zwier@purdue.edu

Abstract: The excited-state dynamics of phenylvinylacetylene (1-phenyl-1-buten-3-yne, PVA) have been studied using laser-induced fluorescence spectroscopy, ultraviolet depletion spectroscopy, and the newly developed method of ultraviolet population transfer spectroscopy. Both isomers of PVA (*E* and *Z*) show a substantial loss in fluorescence intensity as a function of excitation energy. This loss in fluorescence was shown to be due to the turn-on of a nonradiative process by comparison of the laser-induced fluorescence spectrum to the ultraviolet depletion spectrum of each isomer, with a threshold 600 cm^{-1} above the electronic origin in *Z*-PVA and 1000 cm^{-1} above the electronic origin in *E*-PVA. Ab initio and density functional theory calculations have been used to show that the most likely source of the nonradiative process is from the interaction of the $\pi\pi^*$ state with a close lying $\pi\sigma^*$ state whose minimum energy structure is bent along the terminal CCH group. Ultraviolet population transfer spectroscopy has been used to probe the extent to which excited-state isomerization is facilitated by the interaction with the $\pi\sigma^*$ state. In ultraviolet population transfer spectroscopy, each isomer was selectively excited to vibronic levels in the S_1 state with energies above and below the threshold for fluorescence quenching. The ultraviolet-excited populations are then recooled to the zero point levels using a reaction tube designed to constrain the supersonic expansion and increase the collision cooling capacity of the expansion. The new isomeric distribution was detected in a downstream position using resonant-2-photon ionization spectroscopy. From these spectra, relative isomerization quantum yields were calculated as a function of excitation energy. While the fluorescence quantum yield drops by a factor of 50−100, the isomerization quantum yields remain essentially constant, implying that the nonradiative process does not directly involve isomerization. On this basis, we postulate that isomerization occurs on the ground-state potential energy surface after internal conversion. In these experiments, the isomerization to naphthalene was not observed, implying a competition between isomerization and cooling on the ground-state potential energy surface.

I. Introduction

The mechanism of formation of aromatic molecules is important in a variety of contexts ranging from combustion processes to planetary atmsopheres.[1−8] As such, there are many previous studies focusing on reactions that lead from small hydrocarbons to polycyclic aromatic hydrocarbons (PAHs), including studies spanning a wide range of temperatures and pressures, and encompassing hundreds of molecules of different sizes and functional complexity. Titan, one of the moons of Saturn, has a photochemically driven atmosphere rich in hydrocarbons, including benzene, with a wide array of larger PAHs also anticipated. The models of Titan's atmosphere often incorporate radical reactions shared by analogous models of combustion processes, where soot formation could follow similar pathways.[7,9,10]

One of the areas in which both combustion and atmospheric models are still under active development is in the pathways from benzene and its simple derivatives to naphthalene, anthracene, and larger PAHs. Among the postulated pathways are those that utilize a series of hydrogen-abstraction-C_2H_2-addition (HACA) steps,[7,10,11] a recently postulated ethynyl addition mechanism (EAM),[12] and cyclopentadienyl recombination to form napthalene.[13]

In the context of such models, it is important to understand how the aromatic-forming reactions turn on or off depending on the reaction conditions, which can differ substantially between combustion (high *T*, thermally driven), planetary atmospheres (low *T*, intermediate pressures), and interstellar

† Present address: Division of Medical Engineering Research, National Health Research Institutes, 35 Keyan Road, Zhunan 350, Taiwan.

(1) Bauschlicher, C. W.; Ricca, A. *Chem. Phys. Lett.* **2000**, *326*, 283.
(2) Filley, J.; McKinnon, J. T. *Combust. Flame* **2001**, *124*, 721.
(3) Frenklach, M. *Phys. Chem. Chem. Phys.* **2002**, *4*, 2028.
(4) Goldaniga, A.; Faravelli, T.; Ranzi, E. *Combust. Flame* **2000**, *122*, 350.
(5) Roesler, J. F.; de Tessan, M. A.; Montagne, X. *Chemosphere* **2001**, *42*, 823.
(6) Schulz, K.; Hofmann, J.; Zimmermann, G. *Liebigs Ann.-Recueil* **1997**, 2535.
(7) Wilson, E. H.; Atreya, S. K. *Planet. Space Sci.* **2003**, *51*, 1017.
(8) Wilson, E. H.; Atreya, S. K.; Coustenis, A. *J. Geophys. Res. [Planets]* **2003**, 108.
(9) Krasnopolsky, V. A. *Icarus* **2009**, *201*, 226.
(10) Wilson, E. H.; Atreya, S. K. *J. Geophys. Res. [Planets]* **2004**, 109.
(11) Atreya, S. *Science* **2007**, *316*, 843.
(12) Mebel, A. M.; Kislov, V. V.; Kaiser, R. I. *J. Am. Chem. Soc.* **2008**, *130*, 13618.
(13) Marinov, N. M.; Pitz, W. J.; Westbrook, C. K.; Castaldi, M. J.; Senkan, S. M. Modeling of aromatic and polycyclic aromatic hydrocarbon formation in premixed methane and ethane flames; 4th International Congress on Toxic Combustion Byproducts, Berkeley, CA, 1995.

space (very low *T*, few collisions). For example, the recombination of propargyl radicals ($2C_3H_3 \rightarrow C_6H_6$) leads efficiently to benzene in flames[14,15] but are trapped in intermediate C_6H_6 isomer wells under the conditions of Titan's stratosphere.[16] Similar issues are likely to arise in naphthalene formation, where even less is known about the $C_{10}H_8$ potential energy surface and all the various entry ways onto the surface or isomerization pathways once $C_{10}H_8$ is formed. In the context of the photochemical models, one intriguing possibility worth exploring is whether pathways that lead initially to other $C_{10}H_8$ isomers might produce photochemically active $C_{10}H_8$ intermediates that could subsequently undergo photoisomerization to naphthalene.

Such issues form one motivation for the studies reported here. Phenylvinylacetylene (1-phenyl-1-buten-3-yne, PVA) is a structural isomer of naphthalene ($C_{10}H_8$), which was recently identified as a photoproduct of the reaction between UV excited diacetylene (C_4H_2*) and styrene.[17] PVA is also a logical intermediate formed in a variety of ways following formation of benzene or styrene. In fact, PVA has been shown to isomerize to naphthalene in shock tube studies.[6,18]

The molecule is itself composed of two structural isomers, *E*-PVA and *Z*-PVA, in which the phenyl and ethynyl groups are trans or cis, respectively. One question we seek to address is whether either of the two isomers of PVA (*E*- or *Z*-) photoisomerize to form naphthalene under conditions relevant to Titan's atmosphere.

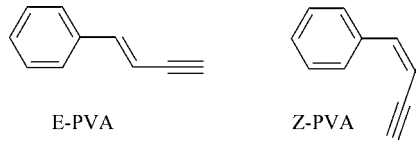

A second motivation for this work is the opportunity it affords to study the state-specific dynamics of photoisomerization. PVA is a close analogue to *cis*/*trans*-stilbene, a molecule that has played a seminal role in the search for vibrationally mode-specific dynamics, and more generally as a large-molecule test case for RRKM descriptions of unimolecular reaction due to the low energy threshold for isomerization in its S_1 state ($\sim$1200 cm^{-1} in *trans*-stilbene).[19−22] In this regard, *Z*-PVA and *E*-PVA form a *cis*/*trans* pair involving even simpler functional groups, with the second phenyl ring of stilbene replaced by an ethynyl group. Our group has recently undertaken a detailed study of the vibronic spectroscopy of *E*-PVA and *Z*-PVA, which serves as the foundation for the present work.[23,24] Unlike stilbene, where one of the isomers (cis) has an unbound excited state, both *E*-PVA and *Z*-PVA have sharp vibronic transitions that can serve as the basis for state-specific studies carried out in both directions, *E*-PVA→*Z*-PVA and *Z*-PVA→*E*-PVA. In both PVA isomers, previous studies show a turn on of a nonradiative process in regions similar to that observed in stilbene. In these studies, it was shown that the most plausible and dominant nonradiative process involved the crossing of the optically accessed $\pi\pi^*$ state with a $\pi\sigma^*$ state involving bending of the C≡CH away from planarity; however, little could be inferred about the role of isomerization in the probed energy regime.[23,24]

In recent years, we have introduced a series of experimental methods that combine isomer-specific laser excitation early in a supersonic expansion with a recooling step prior to interrogation, thereby enabling the isomeric products to be selectively detected downstream in the collision-free region of the expansion.[25−31] These prior studies employed one of two excitation methods, infrared (IR)[25,26] or stimulated emission pumping (SEP).[25,28] Both methods involve excitation of vibrational levels within the first 4000 cm^{-1} of the ground electronic state, necessitating removal of internal energies in this range prior to interrogation. Most of the work to date has thus focused on conformational isomerization[25−29] or cluster photodissociation,[30,31] where the barriers to isomerization or dissociation were less than this amount.

Here, we extend population transfer methods to structural isomerization initiated by ultraviolet (UV) excitation, where absorption of a single photon provides 10 times the energy involved in infrared or stimulated emission pumping excitation. We present a modified version of the population transfer scheme in which a reaction tube appended to the end of the pulsed valve is used to constrain the initial expansion, increasing the number of cooling collisions available to the UV-excited molecule. In what follows, we describe UV-population transfer methods for the first time, and their application to the *E*↔*Z* isomerization of PVA. We use UV-population transfer to determine relative product quantum yields for isomerization as a function of internal energy in the two directions, *E*→*Z* and *Z*→*E*. When combined with laser-induced fluorescence (LIF) excitation and UV-depletion spectra, which determine the relative fluorescence quantum yields of the same bands, a detailed picture of the state-specific isomerization dynamics for PVA is obtained.

II. Experimental and Computational Methods

Ultraviolet population transfer spectroscopy is a double resonance, pump/probe style of experiment (Figure 1) that has been developed as a method for probing isomer-selective excited-state isomerization dynamics. The methodology of UV-population transfer is closely analogous to that of infrared population transfer, which has been used to investigate the ground-state isomerization dynamics of molecules with many conformational isomers.[26,27] However, because the photon energy absorbed by the molecule is nearly an order of magnitude larger than in past work, UV-population transfer spectroscopy must remove much larger amounts

(14) Miller, J. A.; Klippenstein, S. J. *J. Phys. Chem. A* **2001**, *105*, 7254.
(15) Miller, J. A.; Klippenstein, S. J. *J. Phys. Chem. A* **2003**, *107*, 7783.
(16) Newby, J. J.; Stearns, J. A.; Liu, C. P.; Zwier, T. S. *J. Phys. Chem. A* **2007**, *111*, 10914.
(17) Robinson, A. G.; Winter, P. R.; Zwier, T. S. *J. Phys. Chem. A* **2002**, *106*, 5789.
(18) Hofmann, J.; Schulz, K.; Altmann, A.; Findeisen, M.; Zimmermann, G. *Liebigs Ann.-Recueil* **1997**, 2541.
(19) Felker, P. M.; Zewail, A. H. *J. Phys. Chem.* **1985**, *89*, 5402.
(20) Zwier, T. S.; Carrasquillo, E.; Levy, D. H. *J. Chem. Phys.* **1983**, *78*, 5493.
(21) Amirav, A.; Jortner, J. *Chem. Phys. Lett.* **1983**, *95*, 295.
(22) Tahara, T.; Hamaguchi, H. *Bull. Chem. Soc. Jpn.* **1996**, *69*, 925.
(23) Liu, C. P.; Newby, J. J.; Muller, C. W.; Lee, H. D.; Zwier, T. S. *J. Phys. Chem. A* **2008**, *112*, 9454.
(24) Newby, J. J.; Liu, C. P.; Muller, C. W.; James, W. H.; Buchanan, E. G.; Lee, H. D.; Zwier, T. S. *J. Phys. Chem. A*, DOI: 10.1021/jp909243y.
(25) Dian, B. C.; Clarkson, J. R.; Zwier, T. S. *Science* **2004**, *303*, 1169.
(26) Dian, B. C.; Florio, G. M.; Clarkson, J. R.; Longarte, A.; Zwier, T. S. *J. Chem. Phys.* **2004**, *120*, 9033.
(27) Dian, B. C.; Longarte, A.; Winter, P. R.; Zwier, T. S. *J. Chem. Phys.* **2004**, *120*, 133.
(28) Selby, T. M.; Clarkson, J. R.; Mitchell, D.; Fitzpatrick, J. A. J.; Lee, H. D.; Pratt, D. W.; Zwier, T. S. *J. Phys. Chem. A* **2005**, *109*, 4484.
(29) Zwier, T. S. *J. Phys. Chem. A* **2006**, *110*, 4133.
(30) Clarkson, J. R.; Herbert, J. M.; Zwier, T. S. *J. Chem. Phys.* **2007**, *126*, 15.
(31) Zwier, T. S. Laser-initiated isomerization in H-bonded solute-solvent complexes; 230th National Meeting of the American Chemical Society, Washington, DC, 2005.

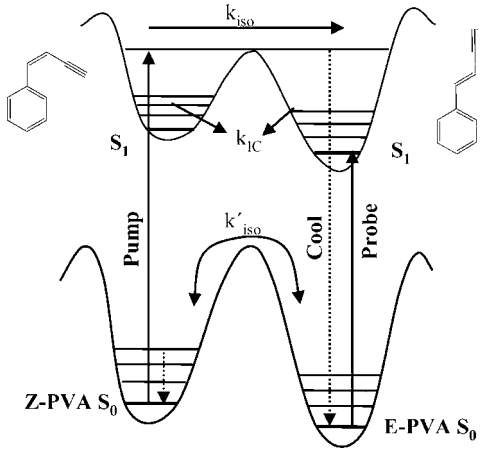

Figure 1. Schematic energy level diagram of the UV-PT experiment illustrating a case where both excited-state and ground-state isomerization can occur, using the *Z* to *E* isomerization of PVA as an example.

of internal energy. To that end, the aforementioned reaction channel has been incorporated so that one can efficiently remove the excess internal energy by constraining the expansion and therefore greatly increasing the number of cooling collisions experienced by a UV-excited molecule.

The experimental setup for UV-population transfer spectroscopy makes use of a Wiley−McLaren type time-of-flight mass spectrometer that has been described in detail previously.[32−34] Samples of *E*/*Z*-PVA are introduced to the ion source region via a pulsed valve (R. M. Jordan) operating at 20 Hz, entrained in helium buffer at a stagnation pressure of 2.7 bar. A 2 mm ID × 2 cm reaction tube was affixed to the end of the pulsed valve (Figure 2), equipped with a ceramic end-plate that minimizes the production of photoelectrons due to the UV laser interaction with the valve face. The effective temperature of gas samples in this reaction tube has been previously estimated to be ∼75 K with pressures of ∼50 mbar, assuming plug flow.[35] Upon exiting the reaction channel, the sample is further cooled by expansion into the vacuum chamber. The free-jet expansion is then crossed by the doubled output of a Nd:YAG pumped dye laser operating in the 300−280 nm region, where the vibrationally resolved, electronic spectra can be recorded using resonant-2-photon ionization (R2PI).

In UV-population transfer experiments, a 20 Hz probe laser is fixed on a intense transition observed in the R2PI spectrum (usually the S_0-S_1 origin band transition), while a 10 Hz pump is tuned through the $S_1 \leftarrow S_0$ region of interest (Figure 3). The difference signal (without vs with the pump laser) is monitored using active baseline subtraction through a gated integrator. However, unlike most double-resonant techniques, the two UV beams are not counter-propagated. Instead, the pump laser is aligned to counter-propagate the expansion axis (orthogonal to the probe beam). In UV-population transfer experiments, the pump laser is timed so that the UV pulse intersects the gas pulse while it is in the reaction tube (pump preceding the probe by ∼65 μs). This allows for cooling back to the zero point level (ZPL) after any isomerization has occurred.

In UV-population transfer experiments (Figure 3a), there are two possible outcomes: (1) population could remain in the reactant well and be recooled to the reactant zero point level (hole-filling) or (2) isomerization could occur, transferring population to a product well

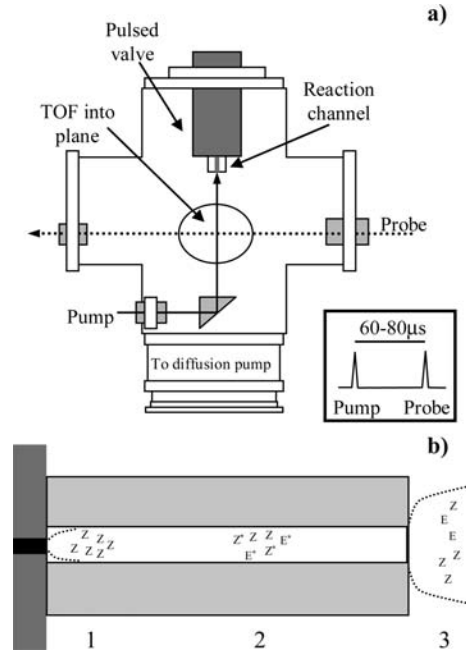

Figure 2. Cross section of the (a) experimental source chamber and (b) reaction channel used in population transfer experiments. Molecules are initially cooled in region 1 as they are expanded into the reaction channel. Selective excitation of an isomer is accomplished by timing the pump laser pulse to intersect the gas pulse while it is still within the reaction channel in region 2. Upon exiting the channel, the isomeric distribution is cooled to the zero point level and enters the collision free region in region 3. The change in isomeric population is monitored downstream in the ionization region via R2PI.

where it is subsequently cooled to the product zero point level, producing a gain in population in that product isomer population. Under hole-filling conditions, the pump laser excites the molecules while they are in the reaction tube, where hundreds of collisions occur. Therefore, the population "hole" created by the pump laser has the opportunity to "fill" via collisional cooling if they do not escape the reactant well. When the probe laser is fixed on a transition out of the zero point level of reactant A, a UV-population transfer scan measures how much of the reactant does not return to the reactant zero point level as a function of pump laser wavelength. When the probe laser is fixed on a transition of the product B, the transfer of population from A to B produces a gain signal that measures how much population is moved into the probed product well.

Alternatively, one can measure where the population is going at fixed pump energy using UV hole-filling spectroscopy. In UV hole-filling spectroscopy (Figure 3b), the pump laser is fixed on a transition of the reactant while the probe laser is scanned through the region of interest. The beam alignment and laser timing conditions are otherwise identical to that used in UV-population transfer. As the probe laser is scanned, a gain (depletion) is recorded whenever the intensity in a transition is increased (decreased) by the pump laser. Ultraviolet hole-filling spectra are used to confirm the selective excitation of the reactant, successful isomerization and recooling of the product, and provide a measure of the relative sizes of depletion and gain signals at a fixed pump excitation wavelength.

Finally, UV depletion spectroscopy (Figure 3b) is another variation of UV−UV double-resonance technique, often used to record conformer/isomer specific UV spectra.[36,37] Previous studies of *E*-PVA and *Z*-PVA used UV hole-burning spectroscopy (Figure 3d) to accomplish this task (in which the pump laser wavelength is fixed while the probe laser wavelength is tuned). Ultraviolet

(32) Arrington, C. A.; Ramos, C.; Robinson, A. D.; Zwier, T. S. *J. Phys. Chem. A* **1998**, *102*, 3315.
(33) Bandy, R. E.; Lakshminarayan, C.; Frost, R. K.; Zwier, T. S. *J. Chem. Phys.* **1993**, *98*, 5362.
(34) Frost, R. K.; Zavarin, G. S.; Zwier, T. S. *J. Phys. Chem.* **1995**, *99*, 9408.
(35) Stearns, J. A.; Zwier, T. S.; Kraka, E.; Cremer, D. *Phys. Chem. Chem. Phys.* **2006**, *8*, 5317.
(36) Michel, P.; Gennet, D.; Rassat, A. *Tetrahedron Lett.* **1999**, *40*, 8575.
(37) Becke, A. D. *J. Chem. Phys.* **1993**, *98*, 5648.

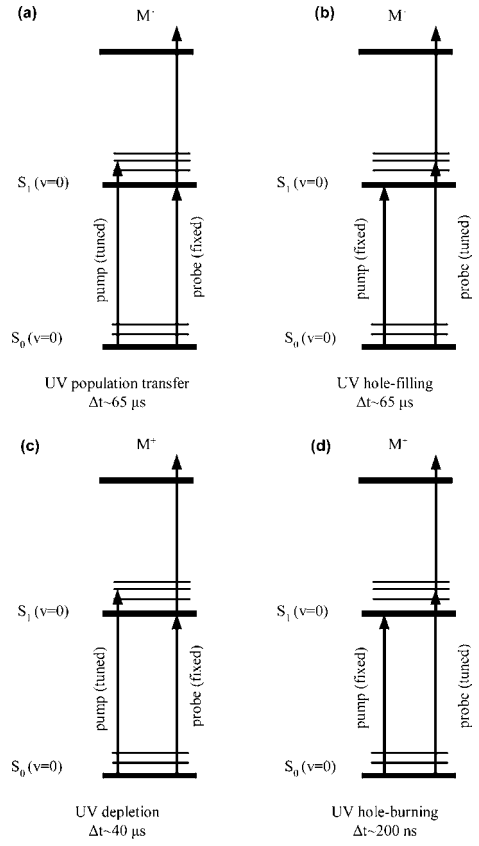

Figure 3. Energy level diagrams for the double resonance techniques used in this work: (a) UV-population transfer, (b) UV hole-filling, (c) UV depletion, and (d) UV hole-burning. In (a) and (b), there are sufficient cooling collisions with the buffer gas for UV excited molecules to recool to the zero point level, while in (c) and (d) no recooling occurs.

depletion spectroscopy does the opposite, fixing the probe laser wavelength on an isomer-specific transition while the hole-burn laser is tuned (Figure 3c). The principal advantage of UV depletion spectroscopy is that one can observe and quantify the absorption intensities of transitions not easily detected in the R2PI spectrum. In the present work, because the pump laser is normally aligned to counter propagate the supersonic expansion, we retain this configuration to obtain mass-selective UV depletion spectra, choosing the delay between pump and probe laser (40 μs) so that the pump laser intersects the gas pulse just outside the reaction channel after the molecules have been fully cooled to the zero point level, in the collision free regime. In so doing, the pump laser intersects all molecules reaching the ion source region, making alignment of pump and probe lasers straightforward.

While described in the case of an R2PI experiment, UV depletion spectroscopy can also be readily carried out utilizing fluorescence detection, as was done recently for *Z*-PVA.[24] Here, we also report fluorescence-based UV depletion spectra for *E*-PVA, acquired using a fluorescence chamber described previously.[27] These spectra will be used to determine relative fluorescence quantum yields for *E*-PVA to compare with those in *Z*-PVA.

E-PVA and *Z*-PVA were synthesized according to the procedure of Michel, Gennet, and Rassat.[24,36] Each isomer of PVA was stored as a dilute solution (<10% in hexane) at 0 °C to minimize polymerization and decomposition. Each isomer was determined be nearly isomerically pure (>90%) by gas chromatography.

To aid in the analysis of the isomerization of PVA, ground-state geometries and harmonic vibrational frequencies were calculated for both isomers using DFT calculations that employed the B3LYP functional[37] at the 6-311+G(d,p) basis set[38] using Gaussian 03.[39] These geometries served as the reference state for configuration interaction singles (CIS)[40] calculations using this same basis set to perform excited-state geometry optimizations, calculate excited-state harmonic vibrational frequencies, and vertical excited-state excitation energies. For comparison, CASSCF calculations[41] were also carried out at the 6-31G(d) basis set[38] using 10 electrons in 10 orbitals to fully represent the $\pi\pi^*$ transition.

Transition state geometries and vibrational frequencies were calculated on the $C_{10}H_8$ ground-state potential energy surface to aid in understanding the barriers to isomerization between *E*-PVA, *Z*-PVA, and naphthalene. Transition states were located using the synchronous transit-guided quasi-Newton method (STQN)[42,43] using B3LYP/6-311+G(d,p) for the ground state.

III. Results and Analysis

A. Review of the Spectroscopy of PVA. Because the population transfer measurements described here build on a foundation of vibronic-level spectroscopy on *E*-PVA[23] and *Z*-PVA,[24] we briefly summarize here those key aspects of that spectroscopy relevant to the present work. Figure 4 compares the laser-induced excitation spectra and S_1 origin single vibronic level fluorescence (SVLF) emission spectra of *E*-PVA (Figure 4a) and *Z*-PVA (Figure 4b). The electronic spectra of both molecules are similar to what is generally seen in other substituted benzenes, with most of the Franck−Condon activity lying in ring and substituent-sensitive modes including ν_1, ν_6, ν_{12}, and ν_{13} (in the Wilson Scheme). The excitation spectrum of *E*-PVA shows vibronic activity up to 1000 cm^{-1}, with a drop-off in intensity above 1000 cm^{-1}. In the absence of wavelength-dependent nonradiative processes, the LIF and S_1 origin SVLF spectra will show similar Franck−Condon activity that reflects the geometry change between these two states (Figures 4a). While this reflection symmetry is apparent in the low-energy region, the LIF excitation scan shows a cutoff in intensity above 1000 cm^{-1} that is not apparent in the SVLF spectrum, indicating a turn-on in nonradiative processes in these higher S_1 vibronic levels.[24] In *Z*-PVA, the LIF excitation spectrum shows an analogous cutoff in fluorescence intensity already 600−700 cm^{-1} above the S_1 origin.

B. Ultraviolet Depletion Spectra. As a first step in probing the excited-state dynamics, Figure 5 presents a comparison of LIF and UV depletion spectra of *E*- and *Z*-PVA acquired using fluorescence detection. The data on *Z*-PVA have been presented previously[24] and are included here for ready comparison with the analogous results on *E*-PVA. Relative fluorescence quantum yields are extracted from the data simply by taking the ratio of the intensities of transitions in LIF ($I_{LIF} \propto N_{exc} \cdot \Phi_f$) to those in UV depletion recorded under otherwise identical conditions ($I_{UVD} \propto N_{exc}$). Because the laser power used in UV depletion is higher than that in a typical LIF spectrum, many transitions in Figure 5 show some degree of saturation compared to the LIF spectrum in Figure 4. Figure 6 overlays on the LIF excitation spectra of the two isomers the relative single vibronic level

(38) Frisch, M. J.; Pople, J. A.; Binkley, J. S. *J. Chem. Phys.* **1984**, *80*, 3265.
(39) Frisch, M. J.; *Gaussian 03*, revision E.01; Gaussian, Inc.: Wallingford, CT, 2004. The full reference is given in the Supporting Information.
(40) Foresman, J. B.; Head-Gordon, M.; Pople, J. A.; Frisch, M. J. *J. Phys. Chem.* **1992**, *96*, 135.
(41) Eade, R. H. A.; Robb, M. A. *Chem. Phys. Lett.* **1981**, *83*, 362.
(42) Peng, C. Y.; Ayala, P. Y.; Schlegel, H. B.; Frisch, M. J. *J. Comput. Chem.* **1996**, *17*, 49.
(43) Peng, C. Y.; Schlegel, H. B. *Isr. J. Chem.* **1993**, *33*, 449.

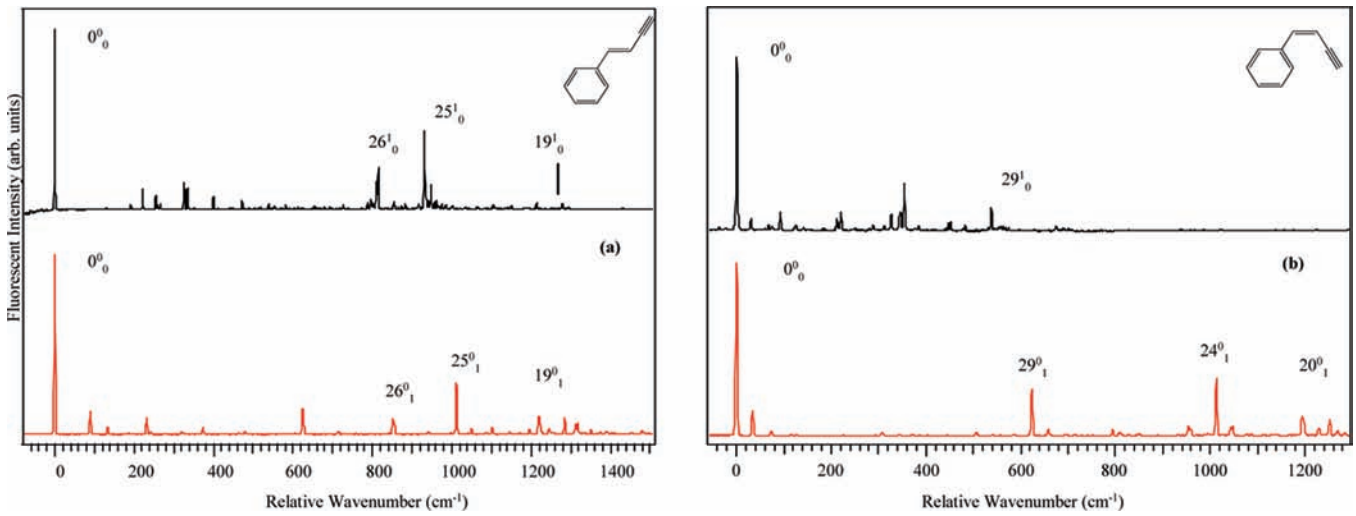

Figure 4. Comparison of the laser-induced fluorescence excitation spectrum (black) and the S_1 origin dispersed fluorescence spectra (red) of (a) *E*-PVA and (b) *Z*-PVA. The loss of reflection symmetry between excitation (black) and emission (red) suggests the turn-on of a nonradiative process in the excited state.

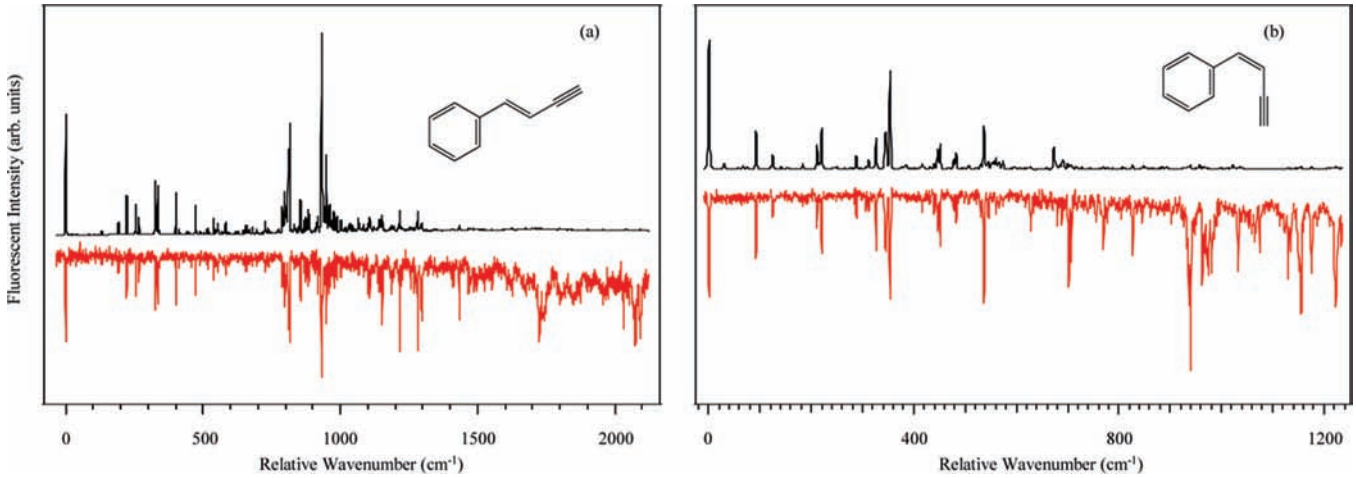

Figure 5. Comparison of the LIF (black) and UV depletion spectra (red) shows a significant decrease in Φ_f above 1000 cm^{-1} in (a) *E*-PVA and above 600 cm^{-1} in (b) *Z*-PVA.

fluorescence quantum yields, Φ_f^{rel}, normalized to 1.00 at the electronic origin.[46] As expected, in both isomers, Φ_f^{rel} shows a precipitous drop by over a factor of 50 as their respective thresholds are overcome. Furthermore, below the threshold, individual transitions show some evidence for mode-specific effects, a point to which we will return in the Discussion.

C. UV Hole-Filling Spectra. A first step in demonstrating the ability to carry out state-specific studies of structural isomerization is to determine whether the experimental scheme shown in Figure 1 can successfully recool the UV excited products to their zero-point levels. Ultraviolet hole-filling spectroscopy (section II) answers this question by fixing the UV wavelength of the pump laser on a transition of the reactant of interest (e.g., *E*-PVA) while the probe laser is scanned through vibronic transitions due to both reactant and product. The middle trace of Figure 7a shows a UV hole-filling scan carried out with the pump laser fixed on the 24^1_0 vibronic band of *Z*-PVA, 933 cm^{-1} above its S_1 origin. LIF scans of *E*-PVA and *Z*-PVA are shown above and below the UV hole-filling scan for direct comparison.

As anticipated, under hole-filling conditions, vibronic transitions arising out of the *Z*-PVA zero point level (Figure 7a) appear as depletions in the UV hole-filling spectrum starting from *Z*-PVA as reactant, as should occur if population is lost from that isomer by UV excitation. At the same time, transitions out of the *E*-PVA S_0 zero point level appear as gain signals, indicating that isomerization from $Z \rightarrow E$ has occurred, and the excess energy has been completely removed by collisions in the reaction channel and postchannel expansion. No other gain or depletion signals appear in this wavelength region, demonstrating that $Z \rightarrow E$ isomerization is being carried out cleanly under UV hole-filling conditions, with recooling complete prior to interrogation. In the same way, the middle trace of Figure 7b demonstrates the reverse isomerization process, from $E \rightarrow Z$ following excitation of the 25^1_0 transition of *E*-PVA, 931 cm^{-1} above its electronic origin. Once again, selective excitation of *E*-PVA and complete removal of excess energy from the UV-excited molecules is apparent.

D. UV-Population Transfer Spectra. Figure 8 shows a series of UV-population transfer spectra carried out on near-pure samples of *E*-PVA (Figure 8a) and *Z*-PVA (Figure 8b) while monitoring the S_0-S_1 origin transitions of the isomer product (top trace) or reactant (middle trace). The bottom trace of

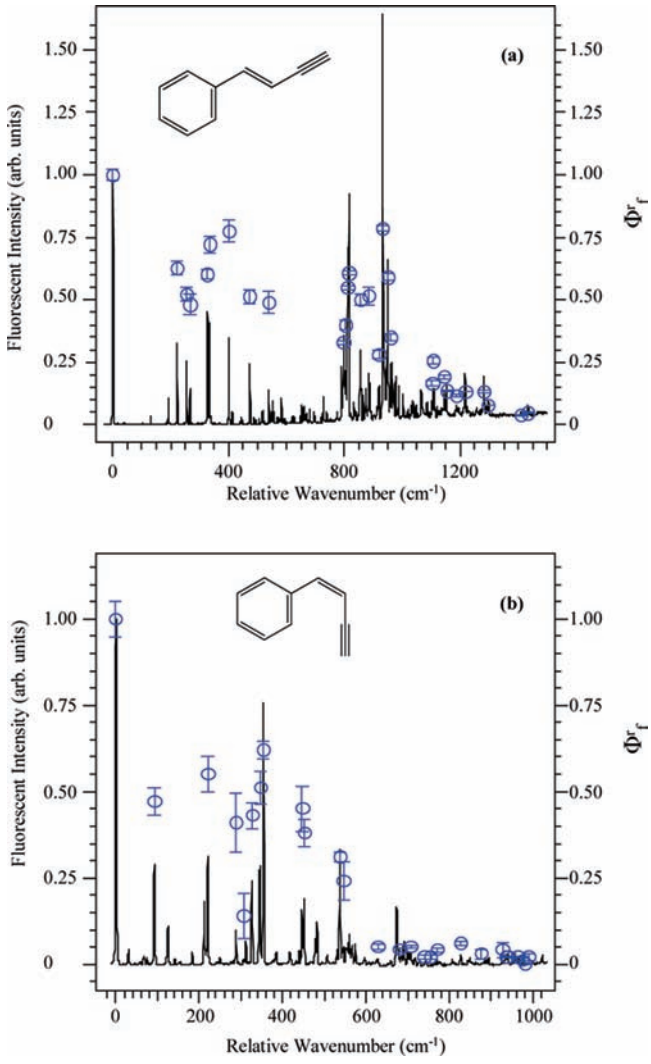

Figure 6. Experimentally observed relative fluorescence quantum yields, with error bars, superimposed on the LIF spectrum for (a) *E*-PVA and (b) *Z*-PVA.

each series is a UV depletion spectrum showing the fraction of the reactant population removed by photoexcitation when recooling of the UV excited molecules does not occur (carried out with R2PI detection). In *E*-PVA, we were able to record the UV-population transfer spectrum from the electronic origin to almost 1500 cm^{-1} above it. In *Z*-PVA, the limited size of our synthesized sample required us to carry out UV-population transfer spectra with pump laser tuned only over the region from 500−1500 cm^{-1} above the *Z*-PVA S_0-S_1 origin.

Several deductions regarding the $E \leftrightarrow Z$ isomerization dynamics can be immediately drawn from these spectra. First, product signal gains are observed in both directions ($E \rightarrow Z$ and $Z \rightarrow E$) already at the S_0-S_1 electronic origin, well below the nonradiative threshold identified by the fluorescence quantum yield measurements.[44] Thus, already at the S_1 origin of both isomers, a fraction of the population undergoes internal conversion to the ground state, leading to isomerization.

Second, in all of the UV-population transfer spectra, a broad background grows in at higher excitation energies, most prominently evident in the product gain spectra. In the $E \rightarrow Z$ UV-population transfer spectrum, the broad feature begins to rise about 715 cm^{-1} above the electronic origin, the same energy region where the fluorescence quantum yield drops. A similar background is evident in the $Z \rightarrow E$ UV-population transfer spectrum (Figure 8b, top trace), with a somewhat less clear threshold, in part because of the extensive hot band structure present in the spectrum. Nevertheless, the rising baseline can be traced back to a similar energy above its S_1 origin (~700 cm^{-1}) as in the $E \rightarrow Z$ case, slightly below the 1000 cm^{-1} nonradiative threshold observed in *E*-PVA. It seems plausible, then, that this rising background is associated with overcoming a barrier to another excited state, which is also responsible for the nonradiative process.

Third, the UV-population transfer spectra monitoring the return to the reactant well ($E \rightarrow E$ in Figure 8a and $Z \rightarrow Z$ in Figure 8b) show small depletions reflecting a small fractional loss in population from the reactant due to isomerization. These spectra follow the intensity patterns in the UV depletion spectra below them, but with reduced intensity due to the partial refilling that occurs under hole-filling conditions. In the following section, we will consider the extent to which these data can be used to obtain isomerization quantum yields. Finally, UV-population transfer spectra monitoring the product show large fractional population changes due to the fact that the initial samples have only a minor impurity of the other isomer, leading to large fractional population changes.

E. Relative Isomerization Quantum Yields from UV-Population Transfer Data. To this point, we have measured relative single vibronic level fluorescence quantum yields for both $Z \rightarrow E$ and $E \rightarrow Z$ isomerization that show a sharp drop at thresholds ~600 and 1000 cm^{-1} above the S_1 zero point level of *Z*- and *E*-PVA, respectively. The UV-population transfer scans of Figure 8 provide qualitative evidence that isomerization occurs both below and above these thresholds. However, we have not yet extracted quantitative values for isomerization quantum yields to determine whether the drop in fluorescence quantum yield is reflected in an analogous turn-on in isomerization quantum yield, that is, whether the nonradiative process funnels population selectively into the product isomer well.

In the previously mentioned studies using IR population transfer spectroscopy, an experimental protocol was developed for measuring absolute isomerization product quantum yields.[26,27] These equations have analogues in UV-population transfer spectroscopy, suitably modified to account for differences in the experimental protocol associated with counter-propagation of the laser and the presence of the reaction channel, with its increased collisional cooling capacity. As detailed in the Supporting Information, these differences make it difficult to extract absolute product quantum yields from the present measurements. As a result, we have chosen instead to report here product quantum yields on a relative scale, normalized to the S_1 origin according to eq 1.[45]

(44) Population transfer at the electronic origin of *Z*-PVA was confirmed by specifically probing that transition in lieu of a full scan near the electronic origin transition.

(45) To make quantitative comparisons to the UVPT spectra, the UVD spectra were retaken under ionization condition and have been found to be nearly identical to those acquired under fluorescence conditions.

(46) Taylor, J. T. *An Introduction to Error Analysis: The Study of Uncertainties in Physical Measurements*; University Science Books: Sausalito, 1996.

$$\frac{\Phi_{AB}(i)}{\Phi_{AB}(0_0^0)} = \frac{I_{AB}^{UVPT}(i)}{I_{AB}^{UVPT}(0_0^0)} \cdot \frac{I_{AB}^{UVD}(0_0^0)}{I_{AB}^{UVD}(i)} \quad (1)$$

These relative isomerization yield measurements are in keeping with our primary interest in determining whether the wavelength-dependent UV-population transfer scans (Figure 8) reflect a turn-on in isomerization quantum yield as the threshold for the nonradiative process is reached.

Table 1 presents relative product isomerization yields for $E \rightarrow Z$ and $Z \rightarrow E$ isomerization for a select set of vibronic transitions of *E*-PVA (left-hand columns) and *Z*-PVA (right-hand columns). These transitions are strong transitions out of the zero point level of each reactant, where we have not included intensity due to the broad background when determining UV-population transfer transition intensities. Error bars were estimated by comparing the area of the transitions from several scans of the UV-population transfer spectrum and propagated using standard methods.[46] The table also includes the measured relative fluorescence quantum yields for the same bands (section III.B and Figure 6) for comparison. It is clear from this comparison that the isomerization quantum yields for these sharp vibronic bands do not change significantly as the fluorescence quantum yield drops by almost a factor of 50. We surmise on this basis that the nonradiative threshold responsible for the drop

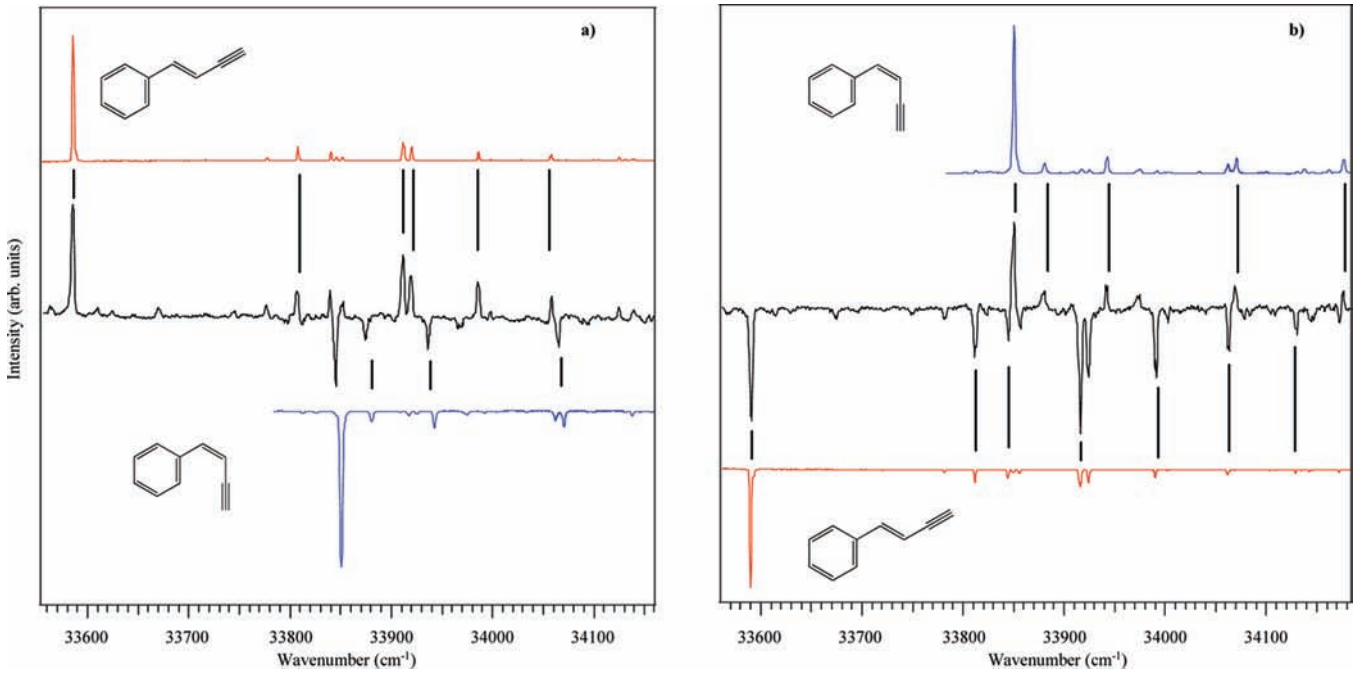

Figure 7. Comparison of LIF spectra (red and blue traces) with hole-filling spectra (red trace) for the (a) $Z \rightarrow E$ and (b) $E \rightarrow Z$ isomerizations. In both panels, the middle spectrum is the UV hole-filling spectrum in which population gain produces an increase in signal and population loss a depletion in signal. The LIF spectrum of the depleted species (blue trace) has been inverted for easier comparison.

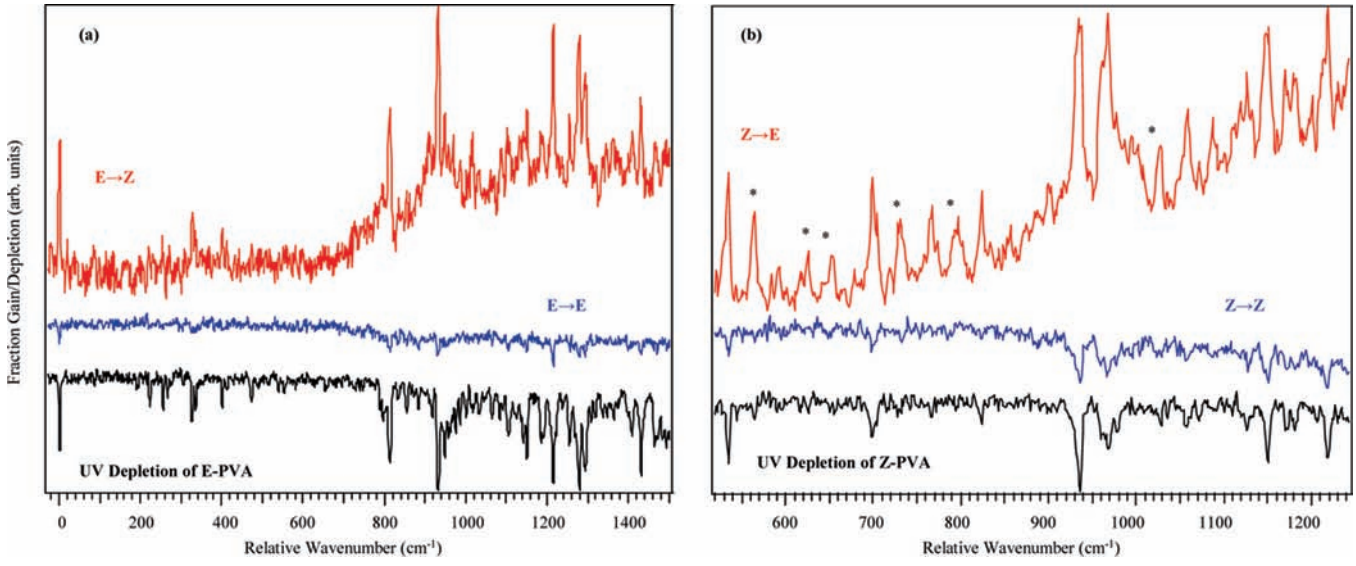

Figure 8. Comparison of the UV population transfer spectra for forming product (red) and reforming reactant (blue) starting from (a) *E*-PVA and (b) *Z*-PVA. The UV depletion spectrum, in which no refilling occurs, is shown in the black trace. Transitions marked with asterisks are assigned to hot-bands of *Z*-PVA present at the temperature in the reaction channel.

Table 1. Comparison of the Fluorescence Quantum Yields with Product Quantum Yields

$\Delta\nu$/cm^{-1}	Φ_f^r (E)[a]	Φ_r (EZ)[b]	$\Delta\nu$/cm^{-1}	Φ_f^r (Z)[c]	Φ_r (ZE)[d]
0	1.00	1.00	0	1.00	
326	0.67	0.77 ± 0.23	535	0.30	1.00
815	0.90	0.90 ± 0.27	702	0.02	1.46 ± 0.44
931	1.26	0.86 ± 0.26	937	0.02	0.95 ± 0.29
1214	0.19	0.96 ± 0.29	967	0.03	1.59 ± 0.48
1279	0.18	0.77 ± 0.23	1060	0.01	1.54 ± 0.46
1292	0.13	0.81 ± 0.24	1152	0.02	1.05 ± 0.32
1434	0.11	0.61 ± 0.18	1223	0.02	1.19 ± 0.36

[a] Fluorescence quantum yields relative to the origin band of E-PVA. [b] Fluorescence quantum yields relative to the origin band of Z-PVA. [c] Isomerization quantum yields relative to the origin band of E-PVA. [d] Isomerization quantum yields relative to the 29_0^1 band of Z-PVA.

in fluorescence quantum yield is not one that is directly associated with $E \leftrightarrow Z$ isomerization. At the same time, additional absorption leading to isomerization produces a broad background that does show a threshold in the same energy region as the drop in fluorescence quantum yield.

F. Ultraviolet Population Transfer Spectra Searching for Naphthalene Products. Because PVA is a structural isomer of naphthalene, it is natural to ask if PVA can photoisomerize to naphthalene. In fact, Zimmer and co-workers reported formation of naphthalene from the flash vacuum pyrolysis of PVA.[6] On the basis of the geometry of the isomers, it would seem most plausible for Z-PVA to isomerize to naphthalene rather than E-PVA, because the acetylenic moiety in Z-PVA is in close proximity to the phenyl ring, as needed for ring closure to occur. To this end, we have tried to observe the photoinduced ring closure from Z-PVA to naphthalene.

To search for naphthalene production, we employed UV hole-filling spectroscopy, where the pump laser was fixed on a vibronic transition of Z-PVA while the probe laser was scanned through the region where a portion of the 1-color R2PI spectrum of naphthalene associated with the S_0-S_2 transition is known to occur (282.5−275 nm).[47] During this search for naphthalene products, many different pump laser frequencies were used, ranging from as far red as the electronic origin of Z-PVA (33 838 cm^{-1}) to as far blue as 4000 cm^{-1} above its S_0-S_1 electronic origin. The population transfer gain signal into the E isomer served as a check that we were still able to transfer population efficiently; however, in no case was naphthalene detected unambiguously. For completeness, the search for naphthalene was also attempted from the E isomer, but again was not detected.

IV. Discussion

A. The Photophysics and Photoisomerization of PVA: Comparison with Stilbene. In the introduction, Z-PVA and E-PVA were posed as close analogues of *cis*- and *trans*-stilbene, a molecule that has served as a prototype for studies aimed at understanding the time scales, reaction pathways, and state-specific energy flow associated with *cis*/*trans* isomerization.[19−21] In stilbene, the excited-state surface accessed from the cis ground state has no bound levels, while the trans isomer has a sharp spectrum with a nonradiative pathway turning on about 1200 cm^{-1} above the trans S_1 origin. An intriguing aspect of the current studies of PVA is that the $\pi\pi^*$ excited-state surface of both isomers (E and Z) is bound, with sharp transitions that

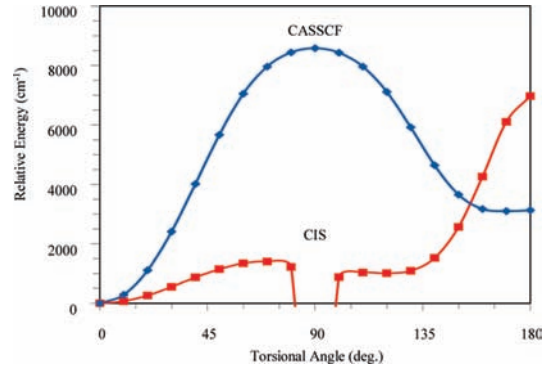

Figure 9. Excited-state potential energy curve for hinder rotation about the double bond in PVA at the CIS and CASSCF levels of theory.

can be used to state-selectively excite and probe both isomers. As a result, the $E \leftrightarrow Z$ photophysics and photoisomerization dynamics can be probed as a function of internal energy from either starting geometry.

In the present work, we have used a combination of LIF, UV depletion, and UV-population transfer spectra to provide relative single vibronic level fluorescence quantum yields and isomerization product yields as a function of internal energy for both E and Z isomers. We are now in a position to pull together our data into a single coherent picture of the excited-state dynamics of PVA.

The relative fluorescence quantum yields show sharp drops beginning 600 and 1000 cm^{-1} above the S_1 origins of Z- and E-PVA, respectively. These thresholds are analogous to the corresponding thresholds in *trans*-stilbene, which have been the subject of ongoing discussions regarding whether the nonradiative rates are governed by statistical or nonstatistical energy flow.[19−22] In PVA, the spectra of both isomers are sharp at the vibronic level below these thresholds, opening the possibility for a quantitative analysis starting from either reactant well. In the present studies, we have not obtained a quantitative measurement of the excited-state lifetime at the S_1 origin, which would be necessary for a complete RRKM analysis. The isomerization quantum yield measurements prove that nonradiative pathways compete with fluorescence already at the S_1 origin. Furthermore, on the basis of the fluorescence decay profile observed in these LIF measurements with nanosecond lasers, we can only place an upper bound on the S_1 origin lifetimes of a few nanoseconds in both isomers. It would be very interesting to have picosecond fluorescence decay profiles or high resolution UV spectra that resolve or partially resolve the rotational structure, which could both be used to deduce the excited-state lifetime.[48] In the absence of that data, one can only estimate the excited-state radiative lifetime on the basis of the calculated oscillator strength for the $\pi\pi^*$ transition. On the basis of the B3LYP 6-311+G(d,p)//TD-DFT/6-311+G(d,p) calculations, we estimate radiative lifetimes of 1.9 and 2.5 ns for the E- and Z-PVA isomers.

Figures 9 and 10 present two different one-dimensional cuts along the excited-state surfaces of E- and Z-PVA. Figure 9 shows a series of single-point calculations projecting up from the ground-state surface, stepping along the C=C twisting coordinate that is the direct analogue of the isomerization coordinate in stilbene. The 0° and 180° end-points are single-

(47) Beck, S. M.; Powers, D. E.; Hopkins, J. B.; Smalley, R. E. *J. Chem. Phys.* **1980**, *73*, 2019.

(48) Alvarez-Valtierra, L.; Yi, J. T.; Pratt, D. W. *J. Phys. Chem. A* **2009**, *113*, 2261.

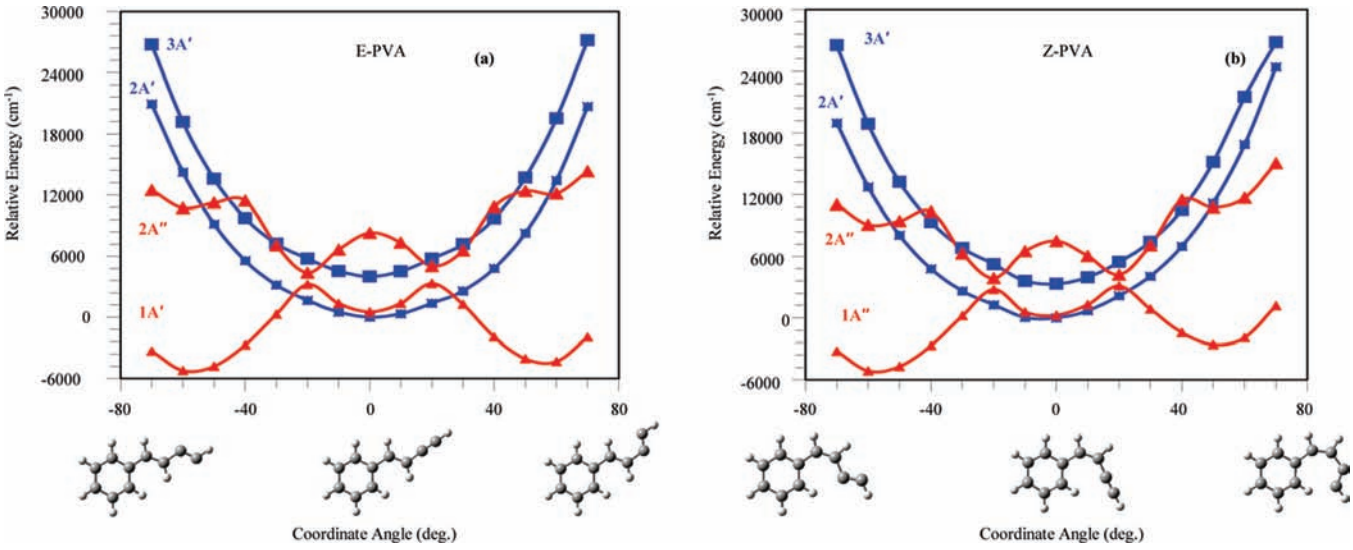

Figure 10. Potential energy surfaces along the acetylenic bending coordinate for the first two excited states of A′ (blue) and A″ (red) symmetry of (a) *E*-PVA and (b) *Z*-PVA.

point projections from the ground-state minima for *E*- and *Z*-PVA, respectively. The CIS calculations become unstable near 90° due to instabilities in the reference state wave function about this geometry; however, the CASSCF calculations show a smooth increase in energy to a transition state about 8500 cm^{-1} above the S_1 origins of *E*- and *Z*-PVA. While this coordinate most closely mimics that in stilbene, it seems unlikely to be responsible for the nonradiative process detected in the first 1500 cm^{-1} above the S_1 origins of *E*- and *Z*-PVA, where isomerization can occur already at the S_1 origin, with a fast nonradiative threshold encountered at energies 10 times smaller than the CASSCF barrier.

Instead, as previously identified in our discussion of the vibronic spectroscopy and fluorescence quantum yields of *Z*-PVA,[24] the acetylenic group is not a passive substituent, but actively participates in the nonradiative pathways in the excited state. Figure 10 presents potential energy curves stepping along the C≡CH bending coordinate, tracking the four lowest energy excited states, two $\pi\pi^*$ states of A′ symmetry and two $\pi\sigma^*$ states of A″ symmetry. The striking result of these calculations is that the lowest energy excited singlet state of PVA is a $\pi\sigma^*$ state of A″ symmetry, with a nonlinear CCH geometry bent ~60° away from linear. In the Franck−Condon accessible region, the lowest $\pi\pi^*$ state is calculated to be slightly lower in energy than the $\pi\sigma^*$ state, but the two are in close proximity over a large range of angles, with crossing points near ±25° in both *E*- and *Z*-isomers. While the absolute magnitudes of the crossing points are somewhat higher (2300/1900 cm^{-1} for *E*/*Z*) than the experimental nonradiative thresholds (1000/600 cm^{-1}), their relative energy ordering is in keeping with experiment. As a result, we postulate that the first $\pi\sigma^*$ singlet state is responsible for the sharp threshold in nonradiative decay in both isomers, a coordinate that is not directly associated with *E*↔*Z* isomerization at all.

This is borne out also by the relative isomerization quantum yield measurements of Table 1. At least for the strong vibronic transitions for which we have quantitatively reliable data, the relative isomerization quantum yields are relatively constant with increasing internal energy, maintaining a similar value above the nonradiative threshold as below it, despite the fact that the fluorescence quantum yields dropped by almost a factor of 50. We conclude that excited-state isomerization is not driving the reduction in fluorescence quantum yield, so that the nonradiative process that turns on in the excited states of *E*- and *Z*-PVA is not the critical bifurcation point for forming one or the other isomer. Instead, the sharp turn-on in nonradiative rate is associated with the surface crossing from $\pi\pi^*$ to $\pi\sigma^*$ states, but the $\pi\sigma^*$ state must itself be an intermediate that facilitates internal conversion to the ground state, with isomerization occurring on the ground-state surface. Furthermore, the close proximity of the $\pi\sigma^*$ state to the $\pi\pi^*$ state in the Franck−Condon region may also mean that this state plays a role in the photoisomerization observed at the S_1 origins of the two isomers, although direct internal conversion to S_0 cannot be ruled out.

Before closing this section of the discussion, two final comments should be made. First, UV-population transfer spectra provide evidence that overcoming the nonradiative threshold accesses a dense manifold of dark states that lead to isomerization, producing the broad backgrounds observed (Figure 8). These background states must gain oscillator strength from the $\pi\pi^*$ state, but are hard to distinguish from simple spectral congestion in the UV depletion scans. However, the UV-population transfer spectra show evidence for the onset of this background absorption near the thresholds for nonradiative decay, suggesting that they arise from accessing the $\pi\sigma^*$ state.

Finally, while the isomerization quantum yields show no mode-specific effects, the relative fluorescence quantum yields do show variations somewhat outside the error bars (Figure 6). While not large, they suggest that, even below the barrier, the coupling to the nonradiative $\pi\sigma^*$ intermediate state may have some mode specificity, an issue worth exploring in greater detail, perhaps by high-resolution methods.

B. The $C_{10}H_8$ Potential Energy Surface and Isomerization to Naphthalene. The one-dimensional cuts on the excited-state surfaces shown in Figures 8 and 9 still leave open the question of how isomerization proceeds following internal conversion on the ground-state surface. The recent ab initio study of the ground-state $C_{10}H_8$ surface by Dyakov et al. had a somewhat different focus (the photodissociation pathways of azulene); nevertheless, it included consideration of many minima and transition states on the ground-state surface, including *E*- and

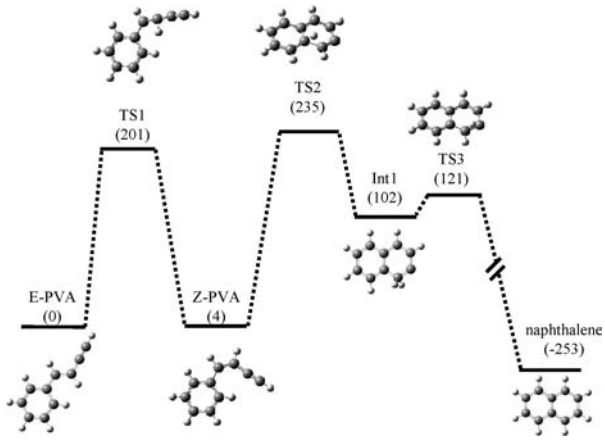

Figure 11. Ground-state potential energy surface for the isomerization from *E*-PVA and *Z*-PVA to naphthalene (kJ/mol) calculated employing the B3LYP function using the 6-311+G(d,p) basis set.

Z-PVA.[49] We have reproduced key aspects of these calculations relevant to the present work at a slightly different level of theory (DFT B3LYP/6-31+G(d)), which are included in Figure 11. As one can see, the calculations predict that the *E*-isomer is more stable than *Z*-PVA by 3.6 kJ/mol. The two isomers are connected by a transition state on the ground-state surface for *E*↔*Z* isomerization, which is 201 kJ/mol above the *E* minimum, well below the energy imparted by UV photoexcitation (660 kJ/mol). This makes clear that, if isomerization is occurring on the ground-state surface, it does so well away from the thresholds probed in UV excitation.

Not surprisingly, the ground-state energy of naphthalene is calculated to be much lower than that of either *E*- or *Z*-PVA (~253 kJ/mol). As Dyakov et al. have pointed out, the pathway from PVA to naphthalene occurs out of the *Z*-PVA well, which is poised for ring closure. According to the calculations, formation of naphthalene occurs via a diradical intermediate that is 98 kJ/mol higher in energy than *Z*-PVA (Figure 11), with barriers into and out of the intermediate well 235 and 121 kJ/mol above *E*-PVA. These energies are only 34 kJ/mol above the barrier for *E*↔*Z* isomerization (201 kJ/mol), also well below the UV photoexcitation energy. Furthermore, the stability of the naphthalene product will greatly favor its formation in the absence of collisional cooling, when the products are under thermodynamic control.

The unsuccessful search for naphthalene products under UV-population transfer conditions indicates that collisional cooling must be fast compared to the time scale for isomerization on the ground-state surface. Under the fast flow conditions in the reaction channel, collisional cooling is complete on the tens of microsecond time scale. In previous experiments in our laboratory on propargyl recombination that employed the reaction channel, the C_6H_6 products formed were shown not to be benzene, indicating that collisional trapping of the C_6H_6 product in other isomer wells must be occurring.[16]

Along the isomerization pathway to naphthalene, we have identified at least one stable intermediate: a biradical species that forms after the initial ring closure, but before the sigmatropic H-atom transfers required to make naphthalene. It is possible that, while the naphthalene product channel is initially energetically accessible, collisional cooling in the reaction channel traps the $C_{10}H_8$ product in an isomer that is optically dark in the region probed (300−275 nm).

V. Conclusions

The isomerization dynamics of *E*-PVA and *Z*-PVA have been studied using the double-resonance techniques of UV depletion and the newly developed techniques of UV-population transfer and UV hole-filling spectroscopy. While *Z*-PVA and *E*-PVA structural isomers are in principle direct analogues of *cis*- and *trans*-stilbene, the presence of the acetylenic group opens up new nonradiative pathways involving a low-lying $\pi\sigma^*$ state that changes the photophysics and photoisomerization mechanisms in fundamental ways. Nevertheless, the ability to state-selectively photoexcite both isomers and follow the isomerization via pump−probe methods such as reported here makes the *E*-PVA↔*Z*-PVA isomerization process a prime candidate for further theoretical studies seeking quantitative descriptions of the intramolecular processes involved. Furthermore, the presence of other important isomerization channels with similar ground-state reaction thresholds, including naphthalene and azulene, makes the *E*-PVA/*Z*-PVA isomers attractive entry points for further studies seeking to understand photoisomerization on this fundamentally important $C_{10}H_8$ potential energy surface.

Acknowledgment. We gratefully acknowledge support from the NASA Planetary Atmospheres program (NNG06GC57G) for this research. We express thanks to Information Technology at Purdue-the Rosen Center for Advanced Computing, West Lafayette, Indiana, for computational resources, H. Daniel Lee for synthetic assistance, and Marek Zgierski for helpful discussion identifying the $\pi\sigma^*$ states as possible causes of the nonradiative thresholds involved. C.W.M. would like to thank the "Deutsche Akademie der Naturforscher Leopoldina" for a postdoctoral scholarship (grant number BMBF-LPD 9901/8-159 of the "Bundesministerium für Bildung und Forschung"). C.-P.L. thanks Taiwan NSC for the financial support through Taiwan Merit Scholarships (TMS-094-2-B-020) during her postdoctoral research at Purdue University.

Supporting Information Available: Extracting quantum yields from UV-population transfer spectra and full ref 39. This material is available free of charge via the Internet at http://pubs.acs.org.

JA908103U

(49) Dyakov, Y. A.; Ni, C. K.; Lin, S. H.; Lee, Y. T.; Mebel, A. M. *J. Phys. Chem. A* **2005**, *109*, 8774.